January, 1984

Directional and dynamic variations ofauroral power spectra related to the ionospheric electron drift velocity

E. Nielsen
C. I. Haldoupis
Bela G. Fejer, *Utah State University*
H. M. Ierkic

JOURNAL OF GEOPHYSICAL RESEARCH, VOL. 89, NO. A1, PAGES 253–260, JANUARY 1, 1984

Dependence of Auroral Power Spectra Variations Upon Electron Drift Velocity in the Eastward Electrojet

E. NIELSEN, C. I. HALDOUPIS,[1] B. G. FEJER,[2] AND H. M. IERKIC[3]

Max-Planck-Institut für Aeronomie

Power spectral observations of auroral electron density fluctuations with a scale length of nearly 1 m have been made with the STARE system (Scandinavian twin auroral radar experiment). Simultaneous measurements of the mean radial Doppler velocities were used to derive estimates of the ionospheric electron drift velocity. The data were analyzed to determine the spectral dependence on the magnitude and direction of the electron drift velocity. The two spectral types, characterized as "narrow" and "broad," were observed simultaneously from the same scattering volume. The width of the broad spectrum (up to about 1200 Hz) can be at least 3 times that of the narrow spectrum. Narrow spectra were observed for both small and large flow angles, while broad spectra were observed only for larger flow angles (typically larger than 70°). Narrow spectra have a width which is insensitive to variations of the flow angle and to variations in the magnitude of the electron drift velocity. The width of the broad spectra, on the other hand, increases rapidly with increasing flow angle and with increasing electron drift velocity. The spectra tend to the asymmetric when the mean line-of-sight Doppler velocity exceeds 350 to 400 m s^{-1}. These observations are discussed in terms of the combined effects of the two-stream and gradient drift instabilities.

INTRODUCTION

Much of our understanding of the physics of electron density fluctuations in the *E* region aurora is based on radar observations, and in particular on Doppler spectral measurements. Almost all auroral spectral measurements in the past were made at frequencies in the range from 40 to 50 MHz corresponding to approximately 3-m irregularities (for references, see *Greenwald et al.* [1975] and *Fejer and Kelley* [1980]). The spectral characteristics change appreciably for different irregularity wavelengths as indicated by UHF auroral observations [e.g., *Moorcroft and Tsunoda*, 1978] and by equatorial multifrequency studies made at 16, 50, and 146 MHz [*Balsley and Farley*, 1971]. In this work we present radar observations made near 140 MHz. The results are therefore relevant for irregularities of nearly 1 m wavelength.

Previous spectral observations of irregularities in a given volume have mostly been made in only one direction. From such measurements it cannot be determined how the characteristics of the irregularities (mean Doppler shift, peak velocity, spectral width, spectral shape, scattering cross section, etc.) depend on the magnitude of the electron drift velocity and on the horizontal angle between the direction of the drift velocity and the direction of observation. Simultaneous spectral measurements from two directions were first made by *Ecklund et al.* [1975] in Alaska using two 50-MHz radars each with a narrow antenna beam, which intersected in a small common volume. Recently, *Sofko et al.* [1982] have reported single-point, crossed-beam measurements made in Canada. In this work we present crossed-beam measurements made in many adjacent locations covering a large area.

Experimental procedure. The observations to be presented were obtained with the Scandinavian twin auroral radar experiment (STARE) system. STARE consists of two pulsed bistatic radars located at Malvik, Norway, and Hankasalmi, Finland. Figure 1 shows the multiple narrow beam pattern of the receiver stations. It is the narrow beams, together with a range resolution of 15 km, which allow Doppler velocity measurements with good spatial resolution over a large area. For a description of STARE, see *Greenwald et al.* [1978]. Figure 2 shows the STARE field of view at 110 km height with about 400 spatial cells (each cell is 0.2° latitude × 0.5° longitude) in which the radars measure both backscatter intensities and radial Doppler velocities. In the present study, in addition to the standard STARE measurements, each radar measured the Doppler spectrum of the received signals in the area shown by the dashed square in Figure 1.

Spectral technique. The power spectra were obtained as the Fourier transforms of the autocorrelation functions of the backscattered signal. The backscattered signals $\chi(t)$ were measured with varying time lags obtained by transmitting a series of 11 double pulses with increasing time spacing τ (from 0.3 ms to 3.3 ms). The measured values were averaged by repeating this pulse scheme about 100 times within the integration time of 30 s. In this way the autocorrelation function $\rho(\tau)$ can be computed,

$$\rho(\tau) = \langle \chi(t)\chi(t+\tau) \rangle \tag{1}$$

In the analysis procedure a standard routine was employed to compute the Fourier transform of the autocorrelation function,

$$F(\omega) = 2\int_0^\infty \rho(\tau) \cos(\omega\tau)\, d\tau \tag{2}$$

The power spectrum $F(\omega)$ is real and ideally positive but, in practice, may be negative for some frequencies because of statistical fluctuations. The frequency resolution is 300 Hz. The power spectra determined in this way have a somewhat overestimated width due to smoothing and spectrum broadening resulting from transforming our rather short data sample.

Doppler spectra are measured in all the grid points inside the large heavy-line square (in Figure 2) which stretches in

[1]Permanently with University of Crete.
[2]Permanently with Cornell University.
[3]Permanently with Arecibo Observatory.

Paper number 3A1485.
0148-0227/84/003A-1485$05.00

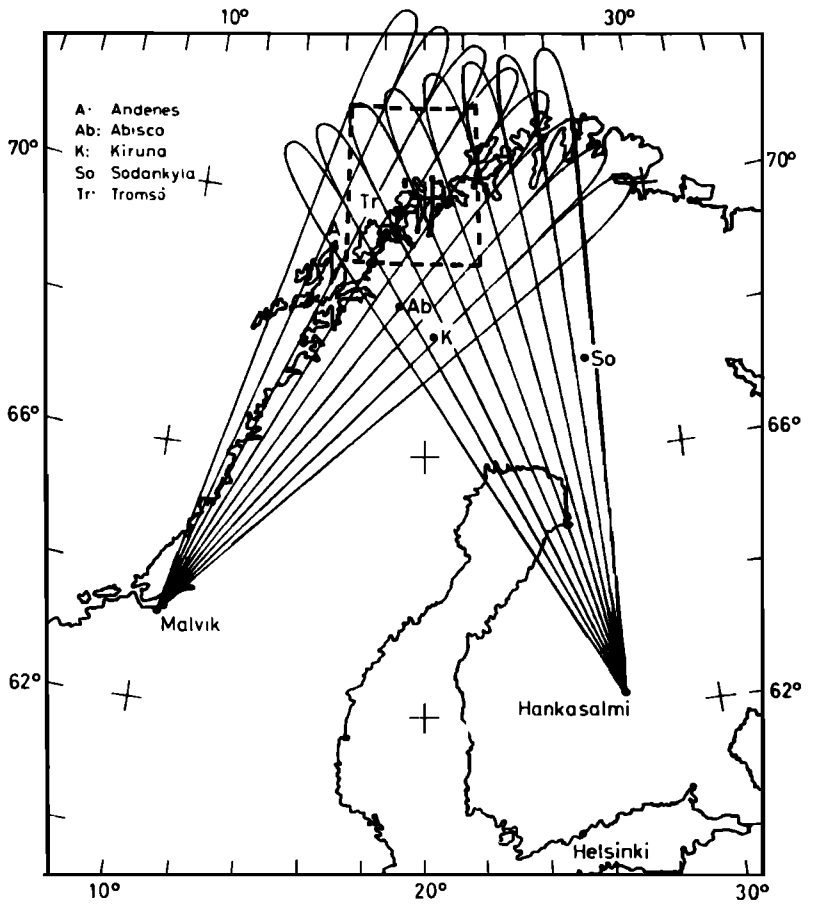

Fig. 1. Map of northern Scandinavia showing the multiple narrow beam pattern of the STARE receiver antennas. In this work we report power spectral observations made inside the dashed square.

latitude from 69°N to 71°N and in longitude from 17°E to 22.5°E. Individual Doppler spectra, corresponding to one grid point and 30-s integration time, are generally reliable when the signal to noise is larger than ~3 dB. To improve spectral stability, we have averaged individual spectra in space and time. Since the purpose of this work is to study the gross spectral features, we deal only with the averaged spectra. Therefore some of the details seen on individual spectra have been smeared out. In the analysis, spatial averages were computed for the six separate areas of 60 × 60 km^2 whose borders are designated by heavy lines in Figure 2. Circles show the central locations within these areas, each composed of nine adjacent grid points. We studied the dominant spectral features and their behavior in time in these six areas.

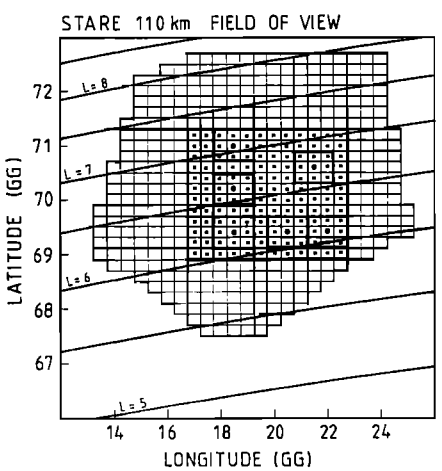

Fig. 2. The STARE field of view displaying the 494 grid cells, in each of which measurements of backscatter intensity and estimates of the electron drift velocity are available. The large square bounded by a heavy solid line contains the grid cells in which power spectra were measured. The small squares bounded by a heavy solid line represent areas over which spatial averages were made.

Drift calculations. We have obtained estimates of the electron drift velocity from the observed radial mean Doppler velocities using both the simple fluid theory and the ion-acoustic approach [*Nielsen and Schlegel*, 1983]. The experimental situation is illustrated in Figure 3, which shows schematically how the phase velocity of the irregularities in the ion-acoustic approach varies as a function of the flow angle. The flow angle θ is defined as the angle between the estimated drift velocity and the radar k vector. The phase velocity is assumed to equal the ion-acoustic velocity C_s for $\theta < \theta_s$ (see

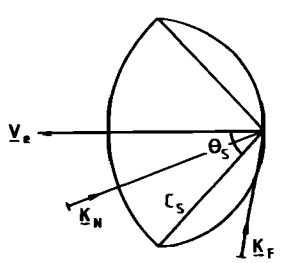

Fig. 3. Schematic illustration of the variations of the irregularity phase velocity in the ion-acoustic approach with respect to the electron drift velocity $\mathbf{V}_E$. C_s is the ion-acoustic velocity; $\mathbf{K}_N$ and $\mathbf{K}_F$ are unit wave number vectors for the two STARE radars; and θ_s is the largest flow angle for which the phase velocity equals C_s.

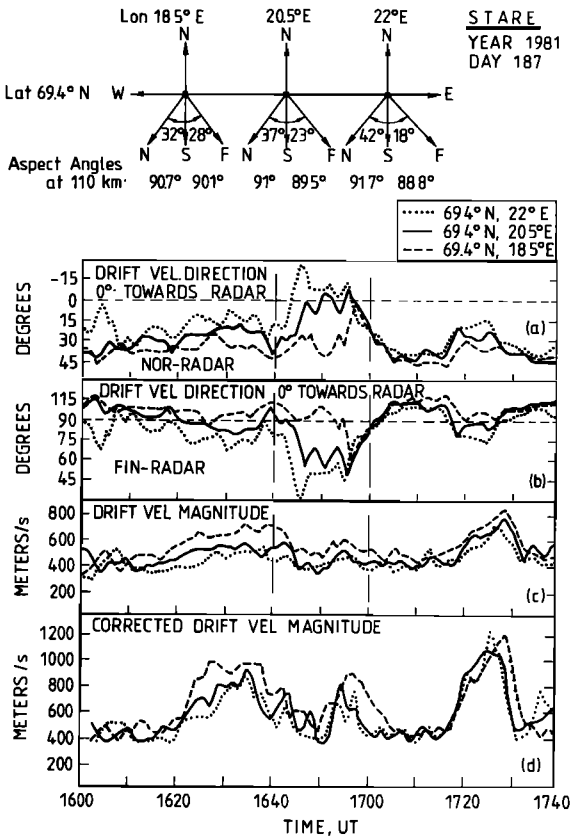

Fig. 4. Estimated electron drift velocity magnitudes and directions for three different locations indicated at the top of the figure.

figure), and to equal the component of the electron drift velocity $\mathbf{V}_e$ for $\theta > \theta_s$. $\mathbf{K}_N$ and $\mathbf{K}_F$ represent the radar K vectors for Norway and Finland, respectively.

In the simple fluid approximation the radial Doppler velocity in a given direction is assumed to be equal to the component of the electron drift velocity $\mathbf{V}_e$ in that direction. Observations from the two radar directions of the radial Doppler velocity components arising from a given volume allow, therefore, derivation of the electron drift velocity. The spectral results will be discussed with respect to these estimates of the electron drift velocities. *Nielsen and Schlegel* [1983] showed that the directions of the estimated velocity vectors were in good agreement with those of the actual drift velocities measured with the European incoherent scatter (EISCAT) radar, but that the accuracy of the estimated magnitude depends on the flow angle θ, as well as on the magnitude of $\mathbf{V}_e$. The best estimates are obtained when θ is large.

Nielsen and Schlegel [1983] also presented evidence that at times a better estimate could be obtained, with the assumption that the irregularity phase velocities in the plasma were limited by the ion-acoustic velocity C_s. In this ion-acoustic approach it is assumed that the radial Doppler velocity equals the ion-acoustic velocity when $\theta < \theta_s$ and equals the component of the electron drift velocity when $\theta > \theta_s$. This latter assumption is used because waves with small phase velocities are probably secondary gradient drift waves which follow a cosine relationship [*Keskinen et al.*, 1979]. On the other hand, the ion-acoustic velocity is also a function of the electric field [*Schlegel and St.-Maurice*, 1981]. Therefore an observation of the radial Doppler velocity for $\theta < \theta_s$ (ion-acoustic velocity in this approach) directly yields the magnitude of the electric field or the electron drift velocity. We call an estimation of the electron drift velocity in this approach a "corrected estimate." The spectral data will also be discussed in relation to these corrected estimates.

Because the simple fluid theory and the ion-acoustic approach represent two extreme interpretations of the observed mean radial Doppler velocities for $\theta < \theta_s$, it is reasonable to expect that the actual electron drift velocity lies in the range estimated from these interpretations.

OBSERVATIONS

The observations to be presented were made from 1600 to 1740 UT on July 7, 1981. The standard STARE data indicated an eastward electrojet with an essentially westward electron drift velocity. Figure 4 summarizes the average characteristics of the mean Doppler velocities measured at three different locations. The locations and line-of-sight geometry for the two radars are shown at the top of the figure. The two upper panels illustrate variations of the flow angles for the two radars. The two lower panels display the amplitude of the

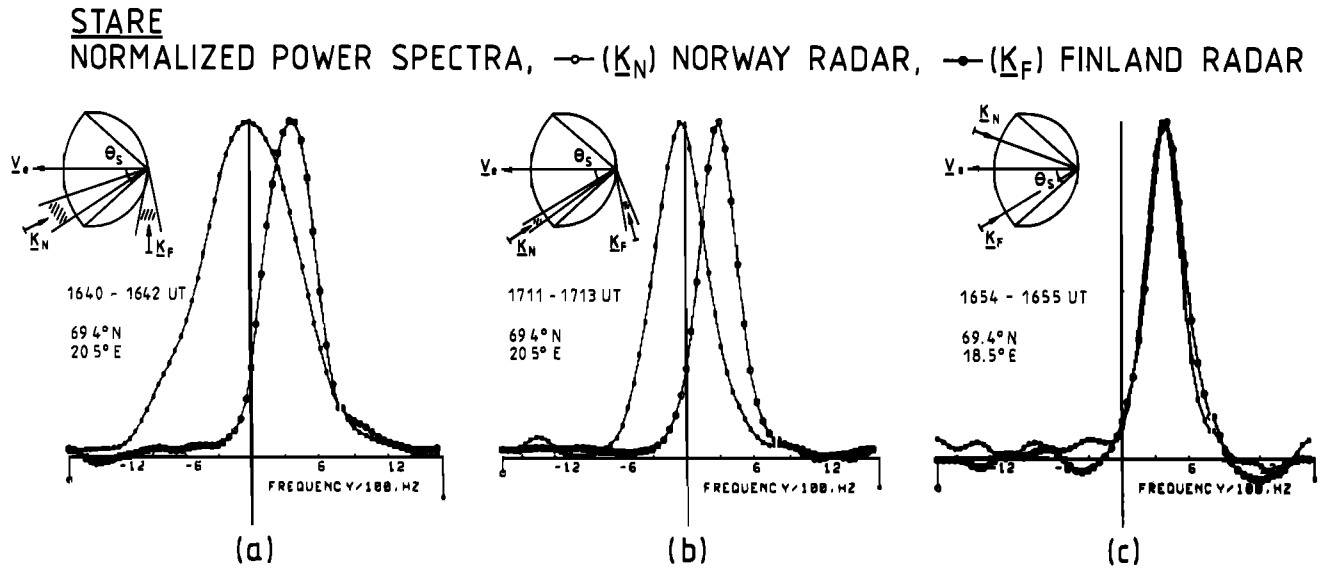

Fig. 5. Examples of symmetric spectra. The geometry of observations is illustrated for each pair of spectra.

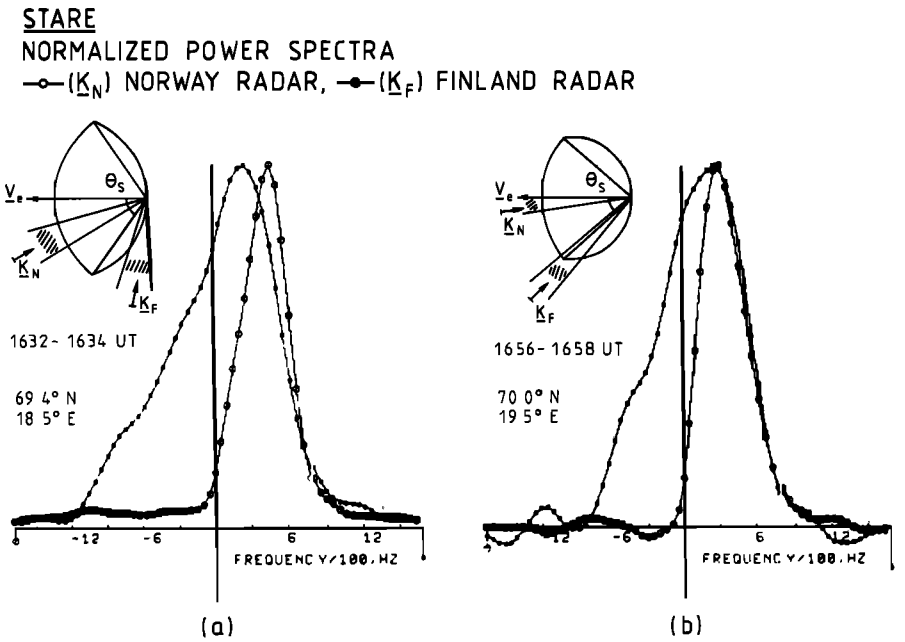

Fig. 6. Examples of asymmetric spectra. The geometry of observations is illustrated for each pair of spectra.

electron drift velocity estimated from the simple fluid theory, as well as the corrected estimates derived with the ion-acoustic approach assuming a backscatter altitude of 110 km. One will notice that the two different interpretations of the observed Doppler velocities mainly differ in that the difference between the minimum and the maximum drift velocity during the given time interval is larger for the ion-acoustic approach (panel *d*) than when the simple fluid theory is used (panel *c*).

Typical spectra. We divided the power spectra into "narrow" and "broad" and into "symmetric" and "asymmetric" spectra. We will show that these spectral characteristics are related to the corresponding flow angle and to the magnitude of the electron drift velocity.

The typical spectra, shown in Figures 5 and 6, are each normalized to their maximum value. The observational geometry, as illustrated in Figure 3, is shown for each pair of spectra.

Figure 5 shows a series of symmetric spectra. Figure 5*a* illustrates a typical pair of symmetric spectra. The westward direction of the electron drift velocity at the time of the observations results in the flow angles shown. In this case, the Finnish radar observed at a flow angle $\theta > \theta_s$, while the Norwegian radar observed at an angle $\theta < \theta_s$. One sees readily that the Finnish spectrum is considerably wider than the Norwegian one. This situation prevails between 1600 and 1620 UT. Figure 5*b* shows a similar case. The main difference, however, is that the spectral width for $\theta > \theta_s$ is comparable with that observed for $\theta < \theta_s$. This situation was observed in the time interval 1705 to 1715 UT, when the flow speed was small and spatially homogeneous (see Figure 4). In Figure 5*c* the spectra from the two radars are nearly identical. This occurred between 1645 and 1655 UT when the flow angles for the two radars were comparable. Notice also that in this case the electron drift speed was small.

Figure 6 shows examples of asymmetric spectra. Figure 6*a* is a typical example of asymmetric spectra observed simultaneously at both radars. In this case also, the spectrum corresponding to the largest flow angle was the widest. The observational situation was similar to that in Figure 5*a*, but the flow speed was typically larger. This type of spectra prevailed

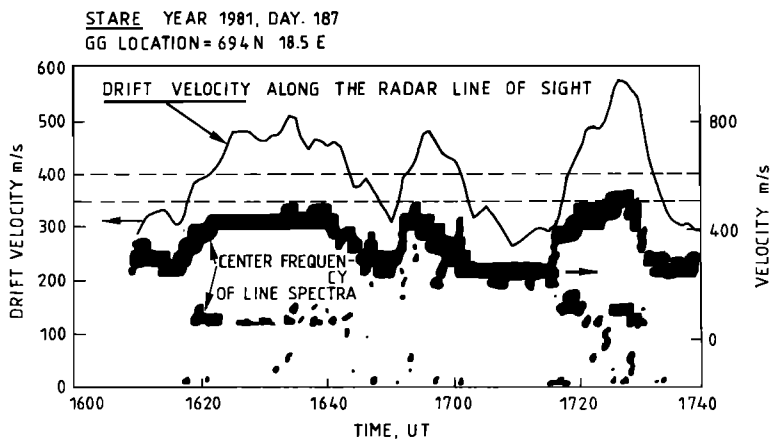

Fig. 7. Comparison of the radial mean Doppler velocity measured from Norway and the center values of the spectral components to which the power spectrum can be resolved. Two spectral components, implying an asymmetric spectrum, tend to occur when the radial drift exceeds 350 to 400 m s^{-1} (see text).

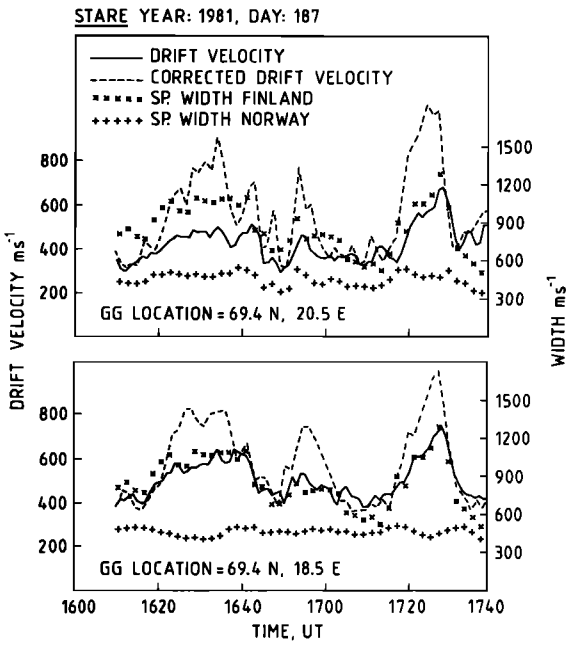

Fig. 8. Two examples of the dependence of the width on the magnitudes of the estimated electron drift velocities. It is clear that the broad spectra (mostly observed from Finland) are very sensitive to variations in the drift velocity magnitude.

between 1620 to 1640 UT and from about 1720 to 1730 UT. Figure 6*b* is a case for which the Norway spectrum for the smaller flow angle is symmetric while the Finland spectrum for the larger flow angle is asymmetric. One notices that the two spectra have peaks at the same frequency and that the Finnish radar has a flow angle close to θ_s in this case. The Finnish spectrum seems therefore to be a composite of the spectral characteristics for $\theta > \theta_s$ (see Figure 5*a* or 5*b*) and $\theta < \theta_s$ (see Figure 5*c*).

In the following sections we examine first the occurrence of symmetric and asymmetric spectra with respect to the magnitude of the mean radial Doppler velocity. Second, we determine the spectral width as a function of electron drift speed and flow angle.

Symmetric and asymmetric spectra. *Whitehead et al.* [1983] analyzed this same data set. The basic question raised in that work was, how good an estimate of the mean Doppler velocity does the double-pulse technique yield? Since the best estimate is obtained when the spectrum is symmetric, this question leads to an analysis of the symmetry of the observed spectra. Several Gaussian power spectra were fitted to the observed spectra, and in addition, the center frequency (or velocity) of the Gaussian spectra was plotted versus time. Asymmetry of the observed spectrum is implied when more than one Gaussian spectrum is needed to fit the data. The center frequencies of the spectra are plotted in Figure 7. Clearly, between 1620 and 1640 UT and between 1720 and 1730 UT, two spectral components are present, one near 100 m s^{-1} velocity and another near 400 m s^{-1}. There is also some tendency for two components between 1655 and 1700 UT. In these intervals the observed power spectra are asymmetric. In this figure it is clear that the spectra tend to become asymmetric when the mean radial velocity exceeds 350 to 400 m s^{-1} (dashed curves in Figure 8).

Spectral width. We used several different procedures to estimate the spectral width. One involved measuring the half-power spectral width directly from the spectra. An estimate of the spectral width was also obtained by using a technique analogous to the computation of the standard deviation. This method, however, overestimates the spectral width if there are significant side lobes in the spectrum. The third method consisted in taking the spectral width as 2 times the standard deviation of a least squares fitted normal distribution to the spectrum after deleting the side lobes. This method was found to be the most satisfactory, and it has been finally adopted here. In this procedure we have excluded the few observed highly asymmetrical spectra. Figure 8 presents two examples

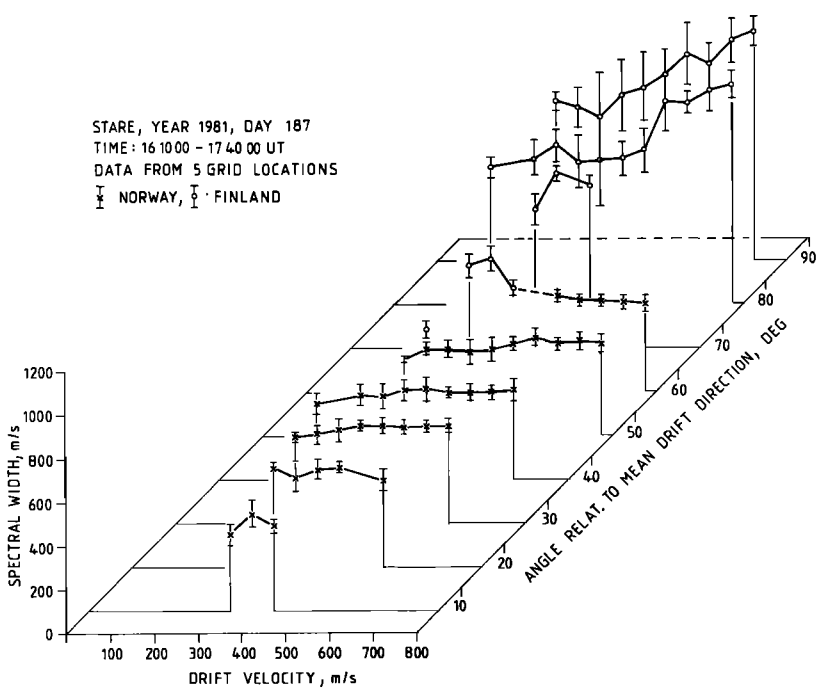

Fig. 9. The power spectral width as a function of the magnitude and direction of the drift velocity relative to the direction of observation (approximately the flow angle).

of the relationship between the spectral width and the electron drift velocity magnitude for both radars at two different grid points. The drift velocity derived in the fluid approach as well as in the ion-acoustic approach is shown. Our analysis revealed that the widths of narrow and broad spectra behave differently. The width associated with narrow spectra is relatively insensitive to drift variations. On the other hand, the width of broad spectra was found to be closely related to concurrent changes observed in the magnitude of the electron drift.

We have also examined the variation of the spectral width with flow angle θ. Negative angles and angles greater than 90° were mirrored into the 0° to 90° range. The narrow spectra have nearly constant widths for a large range of angles (up to nearly 60°), whereas the width of the broad spectra increases with θ and with the magnitude of the drift velocity.

The three-dimensional plot shown in Figure 9 summarizes how the spectral width is related to the electron drift velocity. There is a sharp difference in behavior between the width of narrow and that of broad spectra. Apparently, there is a transitional region somewhere between 55° and 75° where the spectra change from narrow to broad and the width changes from being relatively constant to being proportional to the drift velocity. (Use of the corrected drift velocity is roughly equivalent to changing the scale from 500–800 m s^{-1} to 500–1000 m s^{-1}.) Unfortunately, for the time interval under consideration we did not have sufficient data points to investigate the width behavior in the transitional region. The large deviations seen in the width of the broad spectra are partly due to spatial variations in the electrojet, since we have used six different grid locations (e.g., see Figure 2). The spread in the width at single locations (e.g., Figure 8) was found to be smaller.

In summarizing the experimental results we find the following characteristics of the power spectra of 1-m auroral irregularities:

1. We have observed narrow, broad, symmetric, and asymmetric power spectra. The narrow spectrum is observed usually for small flow angles ($\theta < \theta_s$). It is statistically more stable in space and time than the broad spectrum. On one occasion, when the electron drift velocity was very low ($\sim$350 m s^{-1}), the narrow spectrum was also observed even for $\theta \sim 90°$. The observed half-power spectral width varies between 300 and 600 m s^{-1}. The minimum width of 300 m s^{-1} ($\sim$300 Hz) equals the spectral resolution of the experiment and represents therefore an upper value of this minimum. The width is a weakly increasing function of the electron drift velocity.

2. The broad spectrum is observed only for large flow angles ($\theta > \theta_s$). It can have considerable variations in space and time. The spectral width ranges from 500 to 1200 m s^{-1}, sometimes up to at least 3 times larger than the widths of the simultaneously observed narrow spectra. The width of the broad spectrum is a strongly increasing function of the electron drift velocity.

3. Asymmetrical spectra tend to be observed when the mean radial Doppler velocity exceeds 350 to 400 m s^{-1}. On one occasion an asymmetric spectrum was observed for $\theta \sim \theta_s$ even though the radial velocity was small ($\sim$150 m s^{-1}).

4. Sometimes when both radars observed at a flow angle $\theta < \theta_s$, the two spectra peaked at the same Doppler velocity.

Summarizing, when the drift velocity is low, we find the power spectra to be symmetric and relatively narrow at all flow angles. As the velocity increases, the width increases, slowly for small flow angles ($\theta < \theta_s$) and more rapidly for larger flow angles ($\theta > \theta_s$), and at the same time the narrow spectra become asymmetric. The transition between narrow and broad spectra occurs between the 55° and the 75° flow angle.

DISCUSSION

The spectral characteristics presented in the preceding sections have the same qualitative relationship to the two kinds of estimates we have made of the electron drift velocity. Since these estimates represent extreme cases of interpretation of the observed mean radial Doppler velocity, we conclude that the spectral characteristics are likely to be related in the same way to the actual electron drift velocity.

Radar aurora is associated with two kinds of plasma instabilities in the auroral E layer. It is assumed that the two-stream instability is excited to produce primary irregularities when the radial electron drift velocity exceeds somewhat the ion-acoustic velocity C_s. Thus when

$$V_e \cos \theta > C_s \tag{3}$$

primary two-stream waves are excited [*Farley*, 1963]. Both inside and outside the cone where this inequality is satisfied ($\theta > \theta_s = \arccos (C_s/V_e)$), secondary waves are expected to exist, because of the excitation of the gradient drift instability associated with the primary waves [e.g., *Greenwald*, 1974]. All the Norwegian data in Figures 5 and 6 and the Finnish data in Figure 5*c* are examples of spectra associated with primary irregularities. The Finnish spectra in Figures 5*a* and 6*a* are examples of spectra associated with secondary irregularities.

Although most observations were made either inside or outside the cone, some observations were made close to the cone boundary. The Finnish data in Figure 6*b* are an example of such observations. The spectrum can be viewed as a superposition of a strong narrow spectrum centered at $\sim$350 m s^{-1} and a weaker broad spectrum centered at a somewhat lower radial velocity. Notice that the Norwegian spectrum, which is narrow and observed for a small flow angle, also peaks near 350 m s^{-1}. In the ion-acoustic approach one can interpret the narrow spectral component as characteristic of primary irregularities ($\theta < \theta_s$), while the broad component is associated with secondary irregularities ($\theta > \theta_s$). On the other hand, it is difficult to understand the data in terms of the simple fluid theory. Within that latter framework one would expect the Norwegian spectrum, which was observed at a small flow angle, to peak at a larger Doppler velocity than the Finnish spectrum. Narrow spectra for flow angles less than 50° and broad spectra for flow angles near 90° have also been observed at 50 MHz [*Ecklund et al.*, 1973; *Greenwald et al.*, 1975].

We will show that the different spectral widths of primary and secondary irregularities, the dependence of the width on the electron drift velocity magnitude, and the occurrence of asymmetric spectra are all consistent with the anisotropic backscatter cross section reported in the literature [*André*, 1983; C. Haldoupis and E. Nielsen, manuscript in preparation, 1983]. These authors found the cross section to be highly anisotropic, with its largest value in the direction of the electron drift velocity, and with a broad minimum centered in the direction perpendicular to the drift velocity.

The existence of primary and secondary waves implies turbulence in the backscatter volume. For small flow angles (measured with respect to the mean velocity) the spectrum

would be dominated by backscatter from those regions within the scattering volume, in which the drift velocity points toward or nearly toward the radar. The backscattered signal from other regions would be less significant owing to the anisotropy of the cross section. Thus the spectrum would be dominated by a small range of Doppler velocities and would be narrow.

Moorcroft [1979] points out that the angular spectrum of the secondary irregularities may be complex, since each of the primary waves propagating in the cone defined by (1) will be associated with secondary waves. Because the phase velocity and growth rates of the secondaries is proportional to the relative electron density amplitude $\Delta n/n_0$ of the primaries and the drift velocity V_e [e.g., *Sudan et al.*, 1973, equations 40 and 41], one would expect a relatively large range of phase velocities to exist within the radar beam. The variation of the scatter cross section of secondary irregularities is fairly flat for large flow angles perhaps with a minimum near 90° (C. Haldoupis and E. Nielsen, manuscript in preparation, 1983). All the phase velocities pointing along the radar beam are therefore expected to contribute similar amounts of power to the spectrum. Thus the power spectrum is dominated by a large range of Doppler velocities and becomes broad.

If one assumes that the level of fluctuations, or turbulence, is an increasing function of the velocity, one can also understand the dependence of the spectral width on the electron drift velocity magnitude. The spectrum of primary irregularities is dominated by backscatter from those regions associated with drift directed toward the radar. Thus the spectral width becomes insensitive to the level of turbulence and therefore, according to the assumption, also insensitive to the magnitude of the drift velocity. On the other hand, an increased level of fluctuations would tend to increase the range of velocity components along the radar **k** vector. All these velocities would contribute to the spectrum of secondary irregularities and therefore cause the spectral width to be large, and, according to the assumption, the width would increase with the electron drift velocity (Figures 8 and 9).

A similar insensitivity of the spectral width of primary irregularities to the magnitude of the electron drift velocity was observed at 50 MHz in the equatorial electrojet [*Cohen and Bowles*, 1967; *Balsley and Farley*, 1971]. Observations of equatorial secondary irregularities show variations of the spectral width and drift velocity similar to those reported here [*Balsley*, 1969; *Balsley and Farley*, 1971]. Numerical simulations of secondary irregularities [*Keskinen et al.*, 1979] show that for a fixed wavelength the width of the spectra increases with increasing drift velocity.

The results above imply that the largest Doppler velocities are associated with the strongest backscatter and that the power spectrum therefore should peak near the largest Doppler velocity and decrease with a tail toward lower Doppler velocities. This is consistent with the spectra shown in Figure 6*a*. The narrow symmetric spectra observed at low drift velocities may be a result of the limitation of the experiment. With a spectral resolution of 300 Hz we cannot resolve an asymmetry of these narrow spectra.

Alternatively, the anisotropy may be an effect of a broadening of the backscattering layer in altitude. For a given electron drift velocity the radial phase velocity (or Doppler velocity) decreases with decreasing altitude owing to the variation in collision frequency, while the growth rate of the instability (approximately proportional to backscatter intensity) is expected to maximize near 105 km [*Sudan et al.*, 1973]. If the backscatter region is extended in altitude up to at least 105 km, we would therefore expect the highest Doppler velocities to occur near 105 km altitude and to be associated with the strongest backscatter signal. The observed asymmetric power spectra are likely to be a result of backscatter from a region extended in altitude as well as of an anisotropic backscatter cross section associated with some turbulence.

Unwin and Johnston [1981] reported the simultaneous occurrence of radar backscatter from two layers at distinct altitudes near 105 and 112 km. The spectrum associated with the lower-altitude layer peaked at a lower Doppler velocity than the high-altitude spectrum. The possibility exists that these observations may be the result of the combined effects of a continuous variation in altitude of the phase velocity, as described above, and of a backscatter cross section that peaks at two altitudes, perhaps owing to a double peak in the electron density profile. To investigate this problem and to continue analysis of auroral spectra, joint observations with EISCAT are planned for the future.

We conclude that the spectral characteristics are well correlated with the magnitude of the electron drift velocity and with its direction relative to the directions of observations. These are strong indications that the auroral spectra are governed by the ionospheric electric field. The spectral observations are accounted for qualitatively when we assume that both the two-stream instability and the gradient drift instability are excited and that both produce electron density fluctuations of 1 m scale length in the *E* region. The interpretation is heavily dependent on the anisotropy of the backscatter cross section reported in the literature. Observations at small flow angles are dominated by effects of primary irregularities, while backscatter at large flow angles is dominated by secondary irregularities.

Acknowledgments. The STARE system is operated by the Max-Planck-Institut für Aeronomie in cooperation with the Finnish Meteorological Institute, Helsinki, and ELAB, The Technical University of Norway, Trondheim.

The Editor thanks D. R. Moorcroft and G. J. Sofko for their assistance in evaluating this paper.

REFERENCES

André, D., The dependence of the relative backscatter cross section of 1-m density fluctuations in the auroral electrojet on the angle between electron drift and radar wave vector, *J. Geophys. Res.*, *88*, 8043, 1983.

Balsley, B. B., Some characteristics of non-two-stream irregularities in the equatorial electrojet, *J. Geophys. Res.*, *74*, 2333, 1969.

Balsley, B. B., and D. T. Farley, Radar studies of the equatorial electorjet at three frequencies, *J. Geophys. Res.*, *76*, 8341, 1971.

Cohen, R., and K. L. Bowles, Secondary irregularities in the equatorial electrojet, *J. Geophys. Res.*, *72*, 885, 1967.

Ecklund, W. L., B. B. Balsley, and R. A. Greenwald, Doppler spectra of diffuse radar auroras, *J. Geophys. Res.*, *78*, 4797, 1973.

Ecklund, W. L., B. B. Balsley, and R. A. Greenwald, Crossed beam measurements of diffuse radar aurora, *J. Geophys. Res.*, *80*, 1805, 1975.

Farley, D. T., A plasma instability resulting in field-aligned irregularities in the ionosphere, *J. Geophys. Res.*, *68*, 6083, 1963.

Fejer, B. G., and M. C. Kelley, Ionospheric irregularities, *Rev. Geophys. Space Phys.*, *18*, 401, 1980.

Greenwald, R. A., Diffuse radar aurora and the gradient drift instability, *J. Geophys. Res.*, *79*, 4807, 1974.

Greenwald, R. A., W. L. Ecklund, and B. B. Balsley, Diffuse radar aurora: Spectral observations of non-two-stream irregularities, *J. Geophys. Res.*, *80*, 131, 1975.

Greenwald, R. A., W. Weiss, E. Nielsen, and N. R. Thomson, STARE:

A new radar auroral backscatter experiment in northern Scandinavia, *Radio Sci.*, *13*, 1021, 1978.

Keskinen, M. J., R. N. Sudan, and R. L. Ferch, Temporal and spatial power spectrum studies of numerical simulations of type II gradient drift instabilities in the equatorial electrojet, *J. Geophys. Res.*, *84*, 1419, 1979.

Moorcroft, D. R., Dependence of radio aurora at 398 MHz on electron density and electric field, *Can. J. Phys.*, *57*, 687, 1979.

Moorcroft, D. R., and R. T. Tsunoda, Rapid scan Doppler velocity maps of the UHF diffuse radar aurora, *J. Geophys. Res.*, *83*, 1482, 1978.

Nielsen, E., and K. Schlegel, A first comparison of STARE and EISCAT electron drift velocity measurements, *J. Geophys. Res.*, *88*, 5745, 1983.

Schlegel, K., and J. P. St.-Maurice, Anomalous heating of the polar *E* region by unstable plasma waves, 1, Observations, *J. Geophys. Res.*, *86*, 1447, 1981.

Sofko, G. J., J. A. Koehler, J. Gilmer, A. G. McNamara, and D. R. McDiarmid, Radio auroral magnetic and streaming aspect sensitivities observed on 6 simultaneous links at 50 MHz, *Adv. Space Res.*, *2*(7), 149, 1982.

Sudan, R. N., J. Akinrimsi, and D. T. Farley, Generation of small-scale irregularities in the equatorial electrojet, *J. Geophys. Res.*, *78*, 240, 1973.

Unwin, R. S., and P. V. Johnston, Height dependence in the power spectrum of diffuse radar aurora, *J. Geophys. Res.*, *86*, 5733, 1981.

Whitehead, J. D., H. M. Ierkic, and E. Nielsen, Splitting and divergence of "STARE" auroral radar velocities, *J. Geophys. Res.*, *88*, 2147, 1983.

B. G. Fejer, Cornell University, Phillips Hall, Ithaca, NY 14853.
C. I. Haldoupis, University of Crete, Iraklion, Crete, Greece.
H. M. Ierkic, Arecibo Observatory, Arecibo, PR 00612.
E. Nielsen, Max-Planck-Institut für Aeronomie, D-3411 Katlenburg-Lindau, Federal Republic of Germany.

(Received April 28, 1983;
revised August 15, 1983;
accepted September 9, 1983.)